Oceanologia, 67 (2)/2025, 67201
Polish Academy of Sciences
Institute of Oceanology

https://doi.org/10.5697/NRNG3078

# Water mass stability and mixing in the Banda Sea derived from Global Data Repository and the Jalacitra II Expedition

Noir P. Purba[1,2,*], Noor C.D. Aryanto[2,3], Hendra K. Febriawan[4], Adam B. Nugroho[5], Mohd Fadzil Akhir[6], Afifi Johari[6], Syawaludin A. Harahap[1], Ghelby M. Faid[7], Muhammad H. Ilmi[7], Anom P. Hascaryo[8], Dyan P. Sobaruddin[8], Candrasa S. Dharma[8], Budi Muljana[9], Cipta Endyana[9]

**Abstract**
The dynamics of the Banda Sea can influence larger-scale oceanic processes and contribute to the global ocean circulation system. This research aims to utilize data from a global in situ data repository spanning the years 1960 to 2018, along with data collected from 12 stations during the recent Jalacitra II-2022 expedition. The focus is on analyzing salinity and potential temperature data to construct water mass features, including seasonal temperature-salinity-time diagrams and water column stability using Brunt Vaisala Frequency. Thorpe analysis is employed to investigate turbulent mixing within the region. The results found that temperatures are notably lower in Northwest Monsoon (NWM), reaching 30.0°C, while Southeast Monsoon (SEM) temperatures hover around 28.0°C. Salinity profiles reveal that SEM generally exhibits lower salinity levels, ranging from 33.5 to 34.4, compared to NWM, which ranges from 34.0 to 34.5. Vertical profiles of temperature and salinity variations in the SEM display a more varied thermocline layer depth than NWM. Data from the JC II expedition in the Banda Sea revealed a slight temperature decrease from 27.5°C to 26°C in August, accompanied by salinity variations. Surface salinity was measured at 33.3, while a uniform salinity of 34.6 was observed from 100 meters downward during the same period. This study identifies five dominant water mass types in the Banda Sea, primarily from the Pacific Ocean, which are North Pacific Intermediate Water (NPIW) and North Pacific Subtropical Water (NPSW). During the NWM season, water column instability occurs at depths up to 200 meters, while deeper water column instability is observed during the SEM, extending to a depth of 300 meters, with stability values lower than four cycles/hour. Furthermore, high turbulence generally occurs in the thermocline layer (50 to 300 m).

**Keywords**
T-S time profiles; Ocean stability; Banda Sea; Ocean circulation; Ocean mixing

[1] *Department of Marine Science, Padjadjaran University, Bandung, Indonesia*
[2] *Indonesia National Committee, Intergovernmental Oceanographic Commission (IOC) – UNESCO, Jakarta, Indonesia*
[3] *Research Centre for Geological Resources, National Research and Innovation Agency (BRIN), Jakarta, Indonesia*
[4] *Directorate of Research Vessel Management, National Research and Innovation Agency (BRIN), Jakarta, Indonesia*
[5] *Research Centre for Geological Disaster, National Research and Innovation Agency (BRIN), Jakarta, Indonesia*
[6] *Institute of Oceanography and Environment, University Malaysia Terengganu, 21030 Kuala Nerus, Terengganu, Malaysia*
[7] *KomitmenX Research Group, Padjadjaran University, Bandung, Indonesia*
[8] *Centre for Hydro-Oceanography, Indonesian Navy, Jakarta, Indonesia*
[9] *Department of Geology, Padjadjaran University, Bandung, Indonesia*
***Correspondence**: noir.purba@unpad.ac.id (N.P. Purba)

**Received**: 13 February 2024; **revised:** 11 November 2024; **accepted**: 30 January 2025

## 1. Introduction

Identifying and quantifying the variability and characteristics of water masses are among the most important research topics in the era of climate change (Sprintall et al., 2019). The global ocean is known to have experienced changes in its current patterns and deep-sea warming, which has resulted in a fresher water composition (Johnson and Lyman, 2020).

One of the important global thermohaline passages

in tropical regions is the Indonesian seas (Makarim et al., 2019; Sprintall et al., 2019). The water is transported from the Pacific to the Indian Ocean due to the different sea levels (Katavouta et al., 2022). One of the pathways is the Banda Sea, which has a depth of approximately 7600 m and an area of 470,000 $km^2$. This large-scale circulation of deep ocean currents is driven by temperature and salinity differences (Zhu et al., 2019). As the main path of Indonesian Throughflow (ITF), extensive research has investigated water mass and mixing processes in the Banda Sea region. The Banda Sea serves as a critical pathway connecting the Pacific and Indian Oceans, which plays a vital role in the global-scale circulation patterns, facilitating the exchange of water masses, heat, and nutrients between these two major oceanic basins. These currents interact and generate complex patterns of water circulation, mixing, eddies, and upwelling, thereby resulting in substantial variability in physical and chemical properties (Moore et al., 2003; Purba et al., 2021; Purba and Khan, 2019; Sprintall et al., 2014; Tillinger and Gordon, 2009).

Previous findings have confirmed that the water masses in the Banda Sea primarily originate from the South Pacific Ocean, traversing through the Seram Sea before entering the Banda Sea (Nugraha et al., 2018). Purba et al. (2021) revealed a prevailing southward current direction within numerous straits and seas situated in the Maluku Sea region, with a pronounced direction toward the Banda Sea. Another ITF pathway is through the Mindanao Currents and the Sulu Sea, passing through the Makassar Strait and partially continuing to this region before exiting through the Savu Sea and surrounding areas (Cai et al., 2009; Purba and Damanik, 2021). Additionally, water masses originating from the Indian Ocean and Karimata Strait through the Java Sea contribute to the water mass composition of the Banda Sea as well (Susanto et al., 2010). In addition, the Banda Sea also has complex seafloor topography, such as seamounts, ridges, and trenches. The most recent seamount discoveries were made during the Jalacitra II-2022 "Banda" expedition. The latest insights have been obtained regarding the Nieuwerkerk and the Emperor of China (NEC) Seamounts and several newly discovered seamounts in the vicinity. The peak of these amounts has a water depth of approximately 357 below the surface water (Febriawan et al., 2023).

Despite being a significant component of the global ocean circulation system, the Banda Sea has not yet received adequate research attention, particularly the physical aspects of the water column. Comprehensive studies in this area require regular updates. Changes in oceanic conditions within the Banda Sea, such as sea surface temperature, currents, and atmospheric interactions, can have far-reaching impacts on regional and global climate variability. Furthermore, understanding the dynamics of the oceanographic system in this region is crucial due to its significant impact on biotic ecosystems and abiotic systems (Gusviga et al., 2021). The dynamics of the Banda Sea contribute to our knowledge of climate dynamics and predictions on a broader scale.

Temperature and salinity are important physical parameters of the thermohaline circulation, which influences the thermal mixing and dynamic structural characteristics of the ocean (Balsamo et al., 2018). Despite having challenges in getting the large spatio-temporal resolution of the in-situ data, however, the intensive measurements of physical and biological data have been ongoing since 2000, utilizing various instruments such as Argo floats, ocean gliders, and drifters deployed in the global ocean (Atmadipoera et al., 2019; Purba et al., 2021). By utilizing the available in-situ dataset, this study combines data from the World Ocean Database (WOD-18) with data obtained from the Jalacitra II-2022 (JC II) "Banda" expedition, which was organized by the *Centre for Hydro-Oceanography, Indonesian Navy* (Pushidrosal), to monitor the spatial-temporal temperature and salinity in the Banda Sea.

This paper is organized as follows: Section two discusses the data sets used in this study, validation, and analysis method. Section three describes the result from time series data, including temperature, salinity, stability, and mixing. Section four discusses variability and examines how the water masses formed and the mechanism. Section five presents conclusions and challenges for future research.

## 2. Method

### 2.1 Geographical area and stations' distribution

The Banda Sea is situated in the eastern part of Indonesia, spanning from area 122°E to 135°E, 1.5°S to 8.5°S (Figure 1). This region is interconnected with the Java Sea, Masalembo Sea, Flores Sea, and Makassar Strait to the west. To the north, it is bounded by the Maluku Sea and Seram Sea, while the Arafura Sea lies in the Papua Tanah Air region. To the south, it is bordered by the regions of West Nusa Tenggara, East Nusa Tenggara, and other islands as a boundary towards the Indian Ocean.

The Banda Sea region is characterized by a complex bathymetry that is mostly deeper than 4000 m and is surrounded by islands. Ocean currents in the Banda Sea mainly originate from the northern and western parts. The water masses in this region mostly come from the Makassar Strait and Halmahera seas (Figure 1: blue line). These ocean currents follow the contours of the landmasses and surrounding islands, flowing southward into the Banda Sea. Additionally, some surface currents circulate back to the northern Pacific (McCreary et al., 2007). In the central region of the Banda Sea, the depths reach a maximum of up to 6250 m, while in the eastern part, the Arafura Seas can have depths of 1000 m.

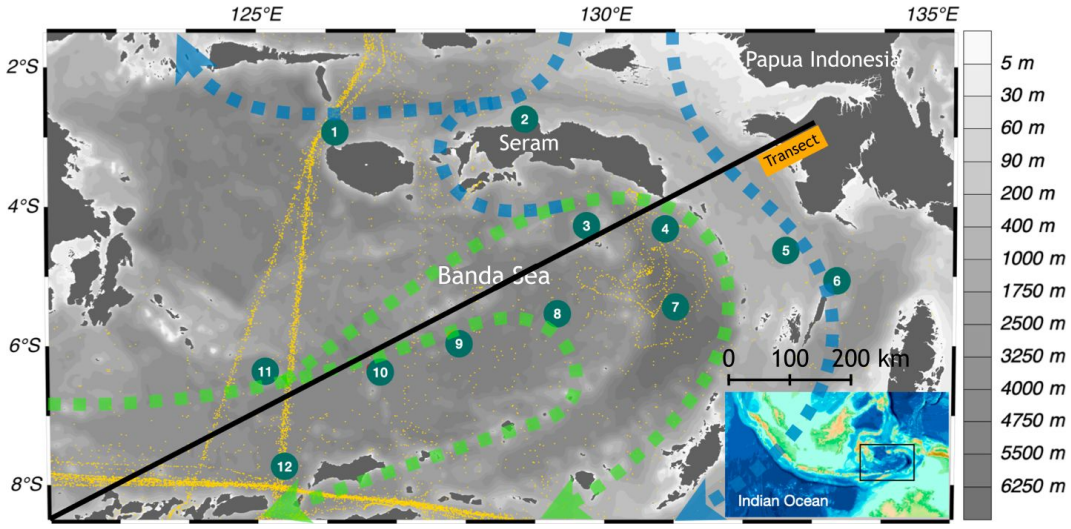


**Figure 1.** The study area of the Banda Sea and its surrounding areas overlaid with ocean depth. Schematic ocean currents with blue dash-line represents annual surface currents from Maluku Seas and Papua Island and green dash-line represent annual surface currents from Makassar and Java Seas (Liang et al., 2019; Zubaedah et al., 2021). The data subset was obtained from the WOD-18 (yellow dots) and JC II-2022 Banda expedition collections (green dots with numbers). Black line indicates the selected transect for vertical distribution observation. This map was processed using Ocean Data View (ODV ver. 5.6.3) software (Schlitzer, 2022).

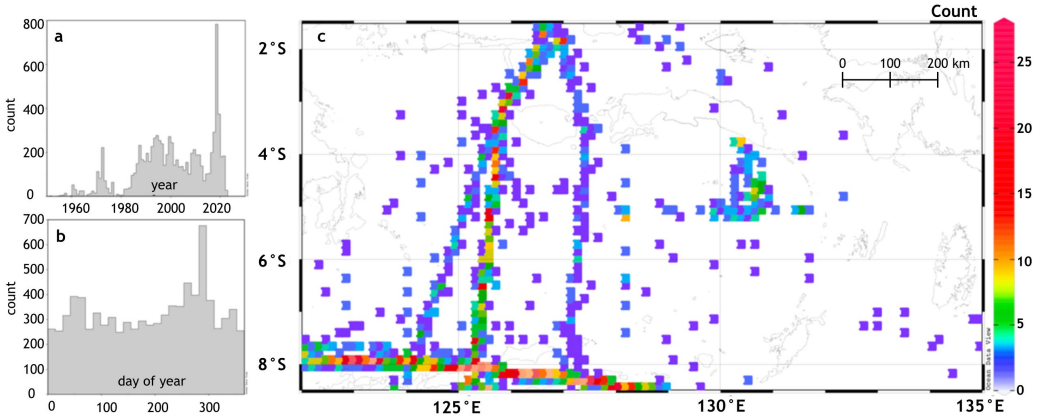


**Figure 2.** (a, b) Temporal distribution range data from the WOD-18 spanning the years 1950 to 2022, demonstrating the availability of data over time, and (c) spatial coverage data, illustrating the extent of the study area.

## 2.2 Data sources

This section summarizes the in situ hydrographic profiles obtained from two primary sources: the World Ocean Database 2018 (WOD-18) global portal data and the recent JC II-2022 Banda expedition (Figure 1 and 2, Table 1). The National Centers for Environmental Information (NCEI) archives provided historical oceanographic data such as temperature and salinity (https://www.nodc.noaa.gov/OCL). This comprehensive dataset comprises information from various WOD-18 projects. It includes high-resolution data collected through a range of instruments, such as CTD (conductivity-temperature-depth) instruments, XBT (expendable bathythermograph) probes, DRB (drifting buoy), PFL (profiled buoy), and MRB (anchor buoy) (Boyer et al., 2018). The dataset was updated every four years, and the latest database was published in September 2018. Detailed information about the updated database can be found in (Boyer et al., 2018).

The Banda Sea expedition (JC II) was conducted aboard the Indonesian Navy's Hydro-Oceanographic Center's vessel (KRI Rigel-933) from April to August 2022. This research collaboration involved researchers from relevant ministries and research agencies, universities, professionals, and private sector entities with marine surveying and geoscience expertise. The primary objective of the fieldwork was to record essential physical and geological parameters that support navigational safety, marine environmental protection, disaster mitigation, and other maritime interests (https://jalacitra.pushidrosal.id). Temperature and salinity measurements were taken using a Seabird

**Table 1.** Data statistic in the three different layers.

| | Min | Max | Mean | Standard Dev. |
|---|---|---|---|---|
| Temperature (°C) | | | | |
| <70 m (mixed layer) | 19.04 | 33.83 | 27.67 | 1.46 |
| 70–150 m (thermocline layer) | 13.5 | 30.29 | 22.43 | 3.05 |
| 150–800 m (intermediate layer) | 2.76 | 29.84 | 9.58 | 3.06 |
| Salinity | | | | |
| <70 m (mixed layer) | 32.17 | 35.07 | 34.17 | 0.26 |
| 70–150 m (thermocline layer) | 32.19 | 34.93 | 34.17 | 0.26 |
| 150–800 m (intermediate layer) | 33.16 | 35.15 | 34.39 | 0.14 |

CTD sensor V19 Plus. The in situ data collection route commenced from the southern Banda, progressed towards the Arafura Sea, and then proceeded northward to the Seram Sea. During the cruise, a total of 13 CTD stations were selected for data collection. However, for this paper, we utilized only 12 stations due to the availability of data. Each station provided comprehensive and reliable datasets that were suitable for the specific objectives of this study.

To support the temperature and salinity data, the surface currents, 600 m, and 1000 m simulations in this study are derived from the Hybrid Coordinate Ocean Model (HYCOM) data in the same period with JC II. Specifically, we utilized the GOFS 3.1:41-layer HYCOM + NCODA Global 1/12° Analysis (NRL) database.

### 2.3 Data processing and quality control

The WOD-18 and JC II expedition datasets consist of in-situ raw data, and for this purpose, the data was filtered to retain only good-quality data. Quality control for this extensive profile dataset is essential to improving the accuracy of the results. Therefore, several steps were conducted before analyzing, as follows:

1. Extracting the required data, including temperature, salinity, oxygen, longitude, latitude, depth, and date in the defined spatial and time range.

2. Identifying outliers and removing data outside the ranges of 0°C to 35°C for temperature, salinity ranges of 20 to 40.

3. Removing stations with less than three values in the vertical direction.

4. Constructing a database from observed levels to standard depths (Purba et al., 2021).

The weighted-average gridding interpolation method was used in scalar values, and XBT/MBT corrections were done using Cheng et al. (2014):

$$\text{estimate} = \frac{\sum_{w_i d_i}}{\sum_{w_i}} \quad \text{where} \quad w_i = e^{-r} \quad \text{and} \quad r = \left(\frac{x}{Lx}\right)^2 \left(\frac{y}{Ly}\right)^2 \tag{1}$$

where $d_i$ represents the weighted average of data points, $w_i$ represents the weighting factor for each data point, $e$ represents the base of the natural logarithm, $r$ represents a normalized distance measure, $x$ and $y$ represent the distance between the point of estimation to the data point along the respective axes, and $Lx$ and $Ly$ are length scales along two axes.

Due to data availability, the temporal range of the data spans from 1 January 1960 to 31 December 2022, and the maximum depth of the data is set at 800 m (Figure 2). The depth range was separated into three distinct layers: the mixed layer (<70 m), the thermocline layer (70–150 m), and the intermediate/constant layer (>150 m), as observed in the Indonesian region (Lana et al., 2017). The thermocline layer is defined as a distinct layer where temperature changes more rapidly with depth compared to the layers above and below. In shallow water, the temperature decreases by 0.2°C, while in deep water, it decreases by 0.8°C from a reference level of 10 meters (Johari and Akhir, 2019; Zeng et al., 2016).

### 2.4 Analysis

Water-mass types by using temperature and salinity profiles were mapped to construct T-S Time (Seasonal T-S) diagrams. These diagrams were created using salinity and potential temperature, which were processed based on TEOS-10 documentation. Furthermore, the classification of water masses followed the methods outlined in previous studies (Emery, 2015; Wyrtki, 1961). Additionally, one zonal section transect was created and analyzed to investigate temperature and salinity dynamics. Furthermore, the stability of the water column was analyzed based on the variable derivation of the Brunt-Väisälä Frequency (BVF), which can be calculated as follows:

$$N = \sqrt{-\frac{g}{\rho 0}\frac{\partial p(z)}{\partial (z)}} \tag{2}$$

where $N$ represents a vertically displaced water parcel that oscillates (cycle $h^{-1}$); $g$ is the acceleration due to gravity (9.8 m $s^{-2}$); $\rho 0$ is the average density of the measurement results (kg $m^{-3}$); $z$ is the depth (positive upward). The $N^2$ was acquired from the absolute salinity and conservative temperature values. For $N$, a value greater than 0 indicates a stable layer and a value lesser than 0 indicates an unstable layer. The calculation of $N^2$ is based on the input of absolute salinity and conservative temperature values, following the method by Jackett et al. (2006). A positive $N^2$

value suggests the presence of a stable water layer, while a negative value indicates an unstable layer. The calculation of the Brunt-Väisälä Frequency involves using vertical density gradients obtained from the TEOS-10 equation of state, which was updated in 2010 (https://www.teos-10.org/). This computation is performed for each standard-depth interval, and the resulting value is assigned to the midpoint of that interval. These midpoint BVF values were projected back to the profile's original pressure (or depth) values using linear least-squares interpolation.

In the investigation of mass mixing in the Banda Sea waters, the estimation of vertical turbulence values was conducted. This estimation measures the turbulent kinetic energy dissipation rate ($\varepsilon$) and vertical eddy diffusivity ($K_\rho$). This study utilized the Optimized Thorpe Method (OTM) to estimate these values, as described in the research conducted by Purwandana et al. in 2020. The calculation/equations used to estimate the turbulent kinetic energy dissipation rate and vertical eddy diffusivity in this method were defined as follows:

$$\varepsilon = \begin{cases} 0.64\, L_T^2 N^3, & \text{dissipation rate when overturn is observed} \\ \max\left(1\times10^{-10}, \varepsilon\left(\frac{N^2}{N_0^2}\right)\right), & \text{background dissipation rate} \end{cases} \quad (3)$$

where $\varepsilon$ represents the turbulent kinetic energy dissipation rate ($m^2\ s^{-3}$), $L_T$ represents the Thorpe Length Scale (m), $N$ represents the buoyancy frequency, $\varepsilon_0\left(\frac{N^2}{N_0^2}\right)$ represents the background dissipation rate (Garrett and Munk, 1975), with a value of $\varepsilon_0 = 7\times10^{-10}\ m^2\ s^{-3}$, which is the canonical GM dissipation rate, and $N_0 = 3$ cph (cycles per hour). The calculation is based on the range of dissipation rates commonly found, which is $10^{-10}$ to $10^{-1}\ m^2\ s^{-3}$. The value of $10^{-10}$ represents the lowest dissipation rate typically observed in calm water locations far from turbulent generation areas.

$$K_\rho = K_{\rho Th-GM} = \Gamma\frac{\varepsilon_{Th-GM}}{N^2} \quad (4)$$

where $K_\rho$ represents the vertical eddy diffusivity ($m^2\ s^{-1}$), $\Gamma$ represents the mixing efficiency, $\varepsilon_{Th-GM}$ represents the Thorpe-Garrett and Munk turbulent kinetic energy dissipation rate (Purwandana et al., 2020).

The analysis incorporates the current velocity variables, which are the Eastward Water Velocity. By integrating the variables, the simulation was able to determine both the speed and direction of the ocean current within the simulation domain. The simulation was done using Parcels, a Python program, which is an acronym for Probably A Really Computationally Efficient Lagrangian Simulator. It comprises Python classes and methods that simplify the creation of particle tracking simulations in aquatic environments (Lange and van Sebille, 2017). Parcels application is specifically designed to operate at the petascale, which denotes a computing system capable of performing at least 1,015 floating point operations per second. This immense computational power allows Parcels to carry out rapid and efficient computations. For this study, the particle type chosen was JITParticle, as it aligns with the research objectives and offers superior computational efficiency compared to ScipyParticle. The particle settings utilized involved the release of one particle from the initial point, utilizing freeslip interpolation. The period lasts for a duration of one month, which starts on the same date as each station and ends 30 days later. The choice to implement a one-month simulation was driven by the need to examine the sea surface currents patterns in the study area. This methodology enabled a thorough analysis required for this study, making it easier to directly compare the variations and/or similarities among the different stations.

## 3. Results

### 3.1 Temperature and salinity profiles

In general, Sea Surface Temperature (SST) and Sea Surface Salinity (SSS) characteristics differ slightly between Northwest Monsoon (NWM) and Southeast Monsoon (SEM). The temperature values during the SEM season tend to be comparatively lower than those recorded during the NWM (Figure 3).

In the NWM season (Figure 3a), temperatures range from 28.5–30.0°C. The lowest temperature in the NWM was found in the southwest of the Banda Sea near the Masalembo Seas (6.5°S, 124.5°E), while the highest temperatures occurred in the western Banda Sea (4°S, 124.7°E). The eastern region (Seram and Aru Sea) was dominated by a temperature of around 29.5°C, while the western region (Buton Island) exhibited more varied temperatures spanning from 28.5–30.0°C. The lowest SST was found in southern Buton Island, while the warmer is in the eastern. In the SEM, the temperature was 26°C in the northern region of the Aru Islands (8°S, 135°E), while its highest reaches 28°C near Buton Island (8°S, 122.5°E) (Figure 3b). The colder temperature conditions were clearly visible in the eastern part near Seram, Wetar, and Aru Sea with values of 26.5–27.0°C. In the western part, adjacent to Sulawesi Island, the temperature values range from 27–28°C. The higher SST is in the northern of Seram Island, with a value of 28°C.

Furthermore, the salinity profile in SEM was generally lower than that of the NWM season. Salinity in the NWM season (Figure 3c) ranges from 34.0–34.5, with the lowest in the northern region around Seram Island (5°S, 131°E) and the highest in the Wetar Island region (8°S, 127°E). Low salinity is also found in the southern island of Buton and the northern region of the Aru Sea, with a value of around 34. During SEM (Figure 3d), salinity ranges from 33.5–34.4, with the lowest value in the eastern (Aru seas) and western region (Buton) with value of around 33.5 and the southwest region, while the highest value was recorded

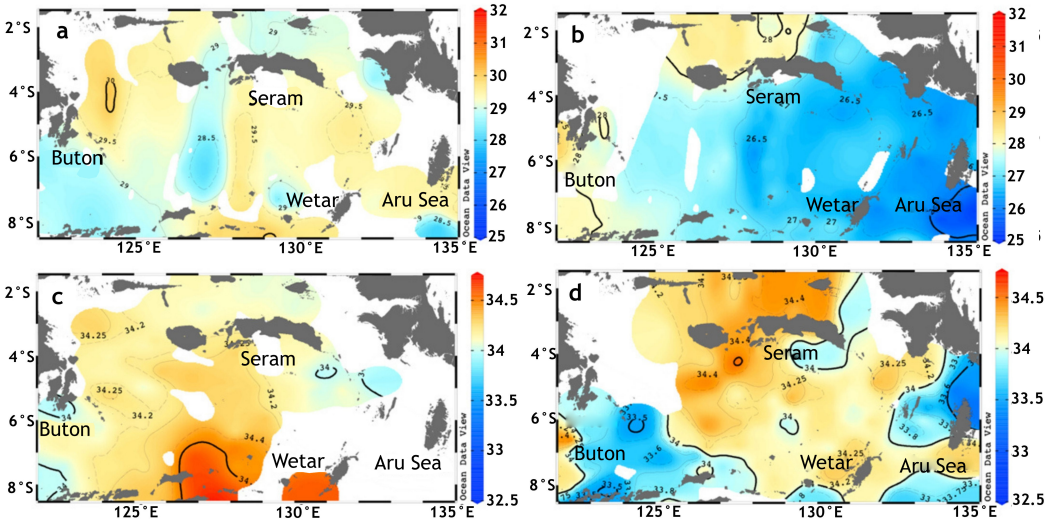


**Figure 3.** The surface profile (color and contour lines) of a) SST in NWM and b) SST in SEM while c) Salinity in NWM and d) Salinity in SEM. Data is provided from WOD-18 and processed using the weighted-average gridding interpolation method with 20 x 20 scale length. White areas indicate no data.

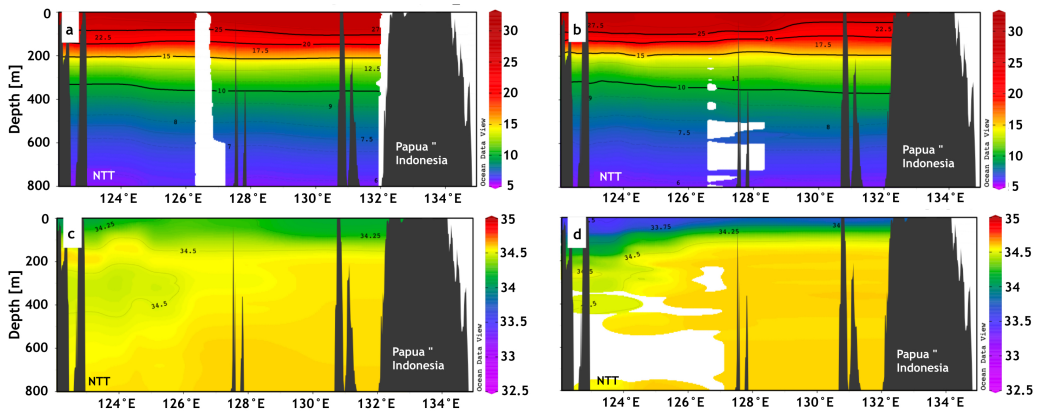


**Figure 4.** Vertical Section of temperature and salinity in both seasons in a transect from NTT to Papua from WOD-18. Temperature profiles in NWM (a) and SEM (b). Salinity profiles in NWM (c) and SEM (d). The weighted-average gridding interpolation with [radius interpolasi] radius was used, with white areas indicating no data.

in the north of Seram Island (34.4). In the southern Aru Sea, the salinity is around 33.7, while in the southern Wetar, the salinity is around 33.8.

Vertical cross-section plots were created to visualize vertical profiles of temperature and salinity variations in the NWM and SEM (Figure 4). These profiles reveal that temperature and salinity in the Banda Sea vary depending on the region and water column layers.

In the NWM (Figure 4a), surface layer temperatures (0–70 m) ranged from 22.5–27.0°C with no significant difference between the eastern (NTT near Wetar) and western regions (Papua Indonesia near Aru Sea). The thermocline layer is identified at a depth of approximately 100 m in the western region (124°E) and 120 m in the eastern region (132°E). Temperature values at 200–400 m depths range from 10–15°C, while temperature ranges from 6–8°C in the deeper layers. In the center of the Banda Sea (around 128°E), the thermocline layer is shallower compared to the eastern and western parts. In the SEM (Figure 4b), the SST ranged from 20–27.5°C, and below the surface, temperature ranged from 10–20°C. Notably, the depth of the thermocline layer in SEM varies compared to NWM. The western region has a deeper thermocline layer than the NWM, which was 120 m, and becomes shallower in the eastern region, which was 90 m. In the deeper layers, temperatures decrease drastically, ranging from 6 to 10°C.

In the NWM (Figure 4c), the salinity profile displayed similar characteristics from the upper water column to 150 m, with values ranging from 34.25 to 34.5. In the lower layers, salinity values differed between the eastern and western parts, with the western part near Wetar Island waters having a lower salinity value (34.5) compared to the east-

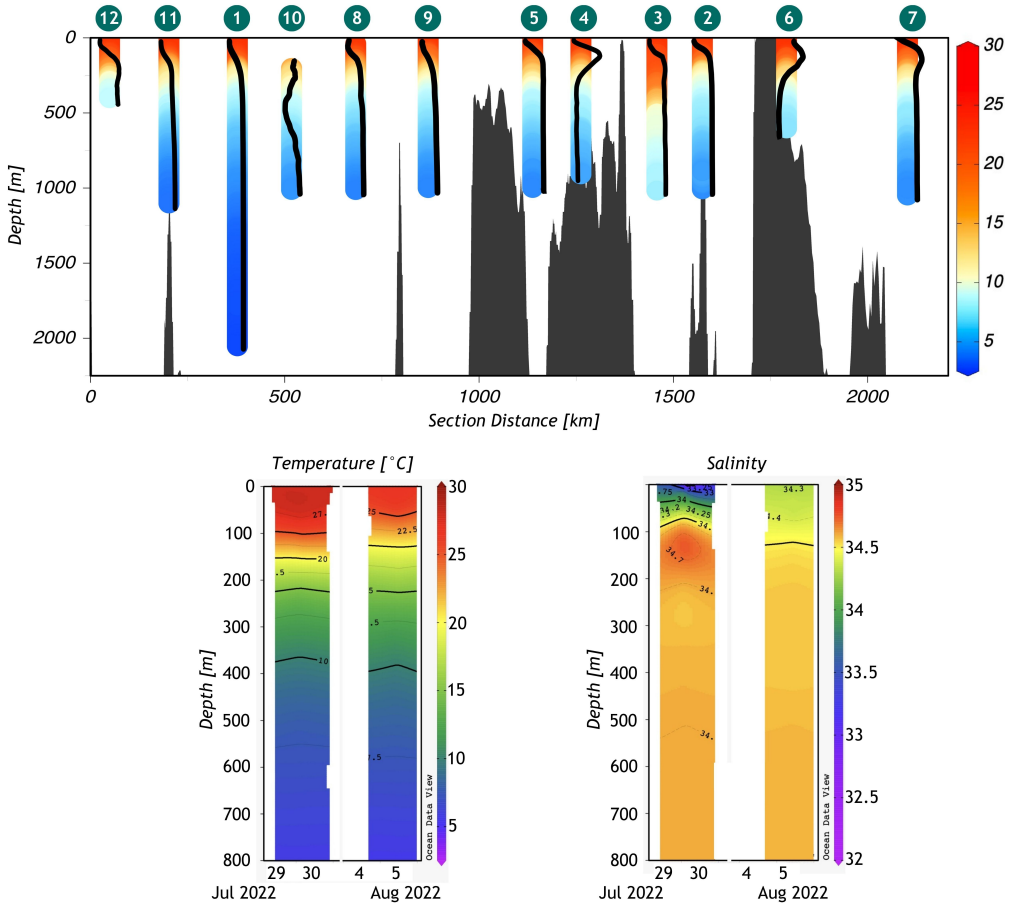


**Figure 5.** Temperature and Salinity Profiles from JC II expedition, (top) colour bars represents temperature and black line represents salinity in 12 stations (bottom) Yo-Yo Casting conducted in station 7 and 8 with colour bar represents salinity and lines represent temperature.

ern waters near Aru Seas (34.7). In this season, a unique profile near the NTT, with a depth of 300–500 m, has a high salinity of around 34.5. In the deepest layer, the salinity values tended to be more homogeneous, around 34.7. During SEM, salinity exhibited depth variations, and small variations occurred in the western regions (Figure 4d). In the western regions, a salinity of 33.7 was observed at a depth of about 100 m, while in the eastern region, it was found to be at a depth of about 50 m. In the layers below, salinity values tended to be more homogeneous, with a salinity value of around 34.5.

Additionally, temperature and salinity measurements in the Banda Sea were also conducted using yo-yo casts during the JC II expedition (Figure 5). The temperature measurements in July indicate that the upper water column had a temperature of 27.5°C, which slightly decreased to 26°C in August. The thermocline layer in July was identified at a depth of approximately 120 m, while in August, it was identified at 100 m. Temperature values become relatively consistent, starting from a depth of 500 m in July and August.

The vertical salinity profile in July displays high salinity variability in the depth range of 0–100 m. The surface water exhibits a salinity of 33.3, which increases to 34.0 at a depth of 50 m. At a depth of 150 m, the salinity reaches 34.7, and it remains uniform from a depth of 200 m onwards. In contrast, during August, the salinity level displays a relatively uniform value. The salinity on the surface is around 34.3 and remains consistent from 100 m downward, with a salinity of 34.6.

### 3.2 Seasonal water mass characteristics

Generally, the water masses were dominated by those originating from the Pacific Ocean. Based on water mass types (Emery, 2015), there are eight dominant water mass types in the study region, including Pacific Equatorial Water (PEW) (7.0–23.0°C, 34.5–36.0), Indonesian Upper Water (IUW) (8.0–23.0°C, 34.4–35.0), Western North Pacific Central Water (WNPCW) (10.0–20.0°C, 34.2–35.2), Indonesian Intermediate Water (IIW) (3.5–5.5°C, 34.6–34.7), North Pacific South Water (NPSW), Eastern North Pacific Central Water (ENPCW) (12.0–20.0°C, 34.2–35.0), Eastern South

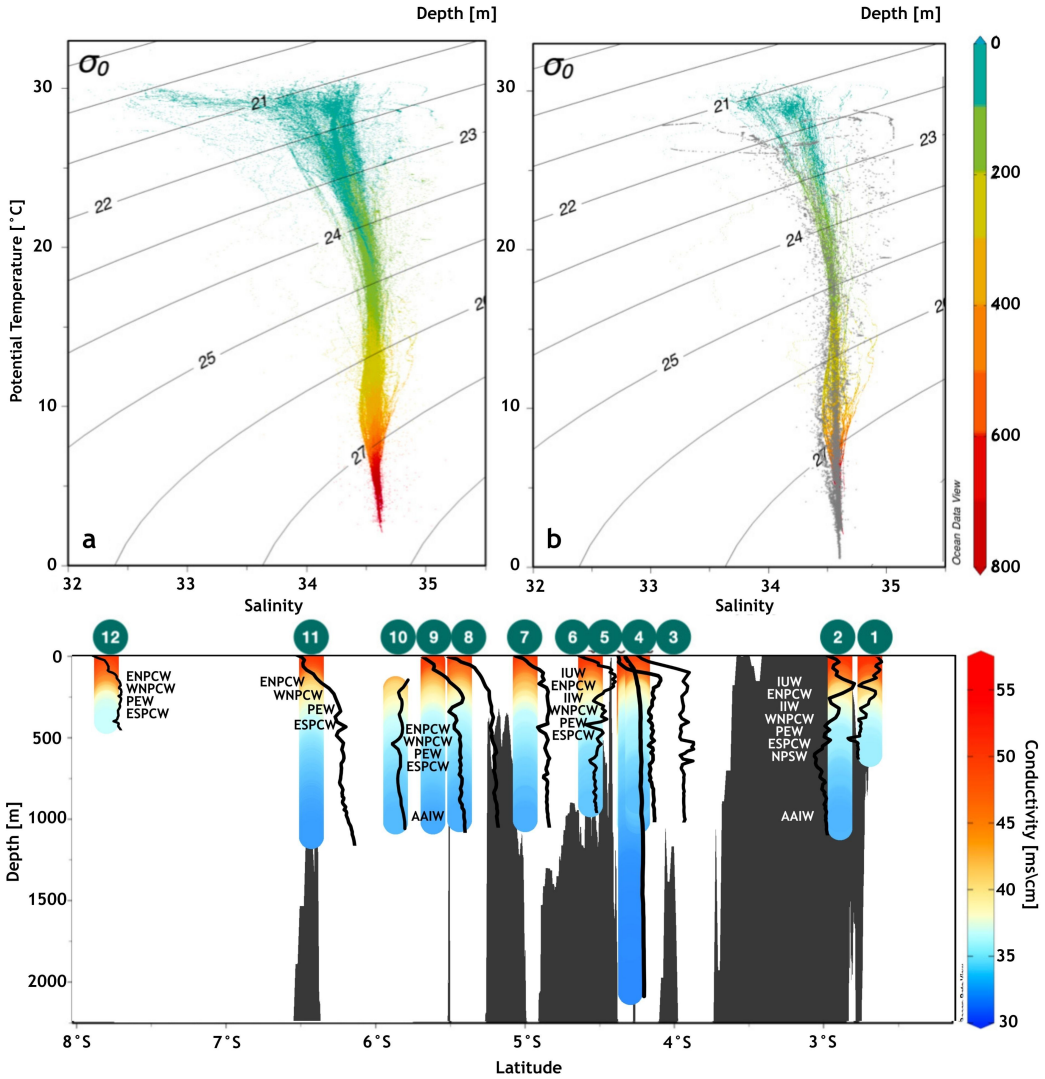


**Figure 6.** Temperature-Salinity Diagram a) in NWM season from WOD-18 and b) in SEM season from WOD-18 18 (colors) and JC II expedition (grey dots), c) detailed description of water masses in each station from JC II expedition.

Pacific Central Water (ESPCW) (8.0–24.0°C, 34.4–36.4) and Antarctic Intermediate Water (AAIW) (2.0–10.0°C, 33.80–34.50) (Figure 6).

The Indonesian Intermediate Water (IIW) and Indonesian Upper Water (IUW) are distinct water masses found at different depths in the Indonesian seas. The IIW is typically observed at a depth range of 700–800 meters, while the IUW is found at shallower depths, ranging from 150–400 m. These water masses play a crucial role in the oceanic circulation and contribute to the overall dynamics of the region. In addition to the IIW and IUW, there are other significant water masses present in the region, which include the Pacific Equatorial Water (PEW) and Eastern North Pacific Central Water (WNPCW), which are typically found at depths ranging from 150–300 m. One notable feature of the Indonesian seas is the observation of the highest salinity north of Seram Island, reaching up to 35.14°C. Conversely, in the intermediate waters, all detected water masses are known to originate solely from the Indian Ocean. This distinction highlights the different sources and pathways of water masses at varying depths within the Indonesian seas. Specifically, within the upper water column, the water mass types detected include the Indonesian Upper Water (IUW) and the Western North Pacific Central Water (WNPCW), both originating from the Pacific Ocean.

### 3.3 Water column stability

The water column stability for both monsoon seasons exhibits apparent disparities between the eastern and western regions. During both monsoon seasons, notable differences were observed in the water column stability across both the eastern and western regions of the study area. These variations extend vertically throughout the water column (Figure 7). During NWM (Figure 7a), water column

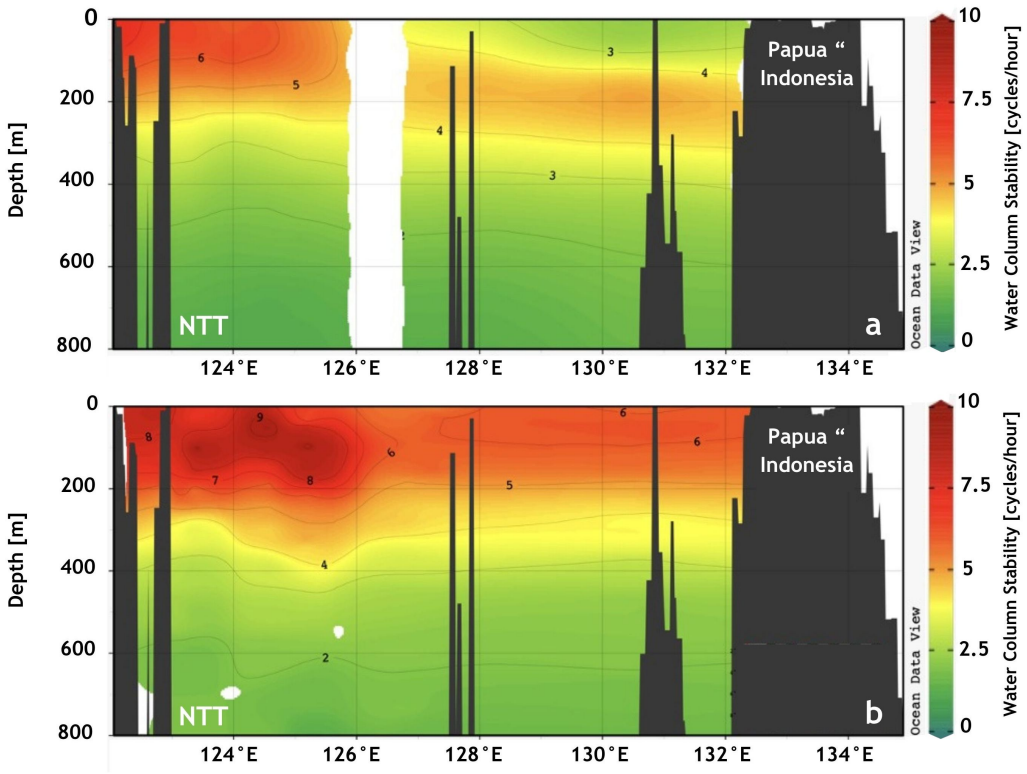


**Figure 7.** Water Column Stability from WOD-18 Data (cycles/hour) in a) NWM and b) SEM.

instability occurs at depths of 0–200 m, and stability sets in from a depth of 200 m with stability values lower than four cycles/hour. The eastern region of the transect exhibits the most distinctive stability pattern, as the surface water column maintains a stability value of 3 cycles/hour, increases to 5 cycles/hour at a depth of 100 m, and then decreases to 4 cycles/hour at a depth of 300 m. In the western region of the transect, the surface water column shows the highest stability value of 6 cycles/hour, twice as it was at the same depth in the eastern transect. In the central Banda Sea (128°E), the stability occurs in the surface and deep water, while in the depths from 50–250 m, it is less stable.

During the Southeast Monsoon (SEM), water column shows deeper instability compared to the NWM, extending to a depth of 300 m and stabilizing thereafter with stability values lower than 4 cycles/hour (Figure 7b). Similar to NWM, the western region of the transect during SEM also displays higher stability values than the eastern region. Stability values during SEM are significantly higher than those during NWM. The stability value in the eastern region of the transect reaches six cycles/hour, increasing to 9 cycles/hour in the western transect region.

### 3.4 Turbulent mixing

The characteristic of mixing in the Banda Sea was determined vertically (~isopycnal) and horizontally showed average dissipation in different layers (Figure 8). Based on the analysis of dissipation rate ($\varepsilon$) and vertical eddy diffusivity $K_\rho$ using OTHORPE in each layer, it was found that high turbulence generally occurs in the thermocline layer (50 to 300 m). In these layers, the value of $\varepsilon$ ranges from $10^{-7}$ to $10^{-6}$ m$^2$ s$^{-3}$, except at stations 7 and 8 (eastern Banda Sea), where low turbulence was observed ($< 10^{-7.5}$ m$^2$ s$^{-3}$). Moreover, high diffusivity was also observed in this layer ($> 10^{-4.5}$ m$^2$ s$^{-1}$), with values $K_\rho$ ranging from $10^{-4}$ to $10^{-2.5}$ m$^2$ s$^{-1}$. In contrast, at greater depths (>300 m), values of $\varepsilon$ and $K_\rho$ indicate low dissipation rates and moderate diffusivity, with values below $10^{-7.5}$ m$^2$ s$^{-3}$ and $10^{-6}$–$10^{-3}$ m$^2$ s$^{-1}$, respectively. Additionally, high turbulence is often observed in regions close to or shaped like straits, as indicated by the values at stations 4, 5 (northern Aru Sea), and 12 (NTT), where significant changes and mass mixing occur in those areas (Figure 9).

Vertically, the dissipation rate profile in the Banda Sea ranges from $10^{-10}$ to $10^{-6}$ m$^2$ s$^{-3}$. High turbulence (>$10^{-7.5}$ m$^2$ s$^{-3}$) occurred in the mixed layer and thermocline at almost all stations except for stations 1 (northern Seram) and 8 (central of Banda Sea). The highest turbulence was observed at station 4 in the thermocline layer (50 to 180 m), with $\varepsilon$ values ranging from $10^{-6}$ to $10^{-5.5}$ m$^2$ s$^{-3}$. This is attributed to the location of station 4 along the path of water mass outflow in the strait. However, at stations 1 and 8, the vertical dissipation rate profile did not detect any turbulence (Figure 10).

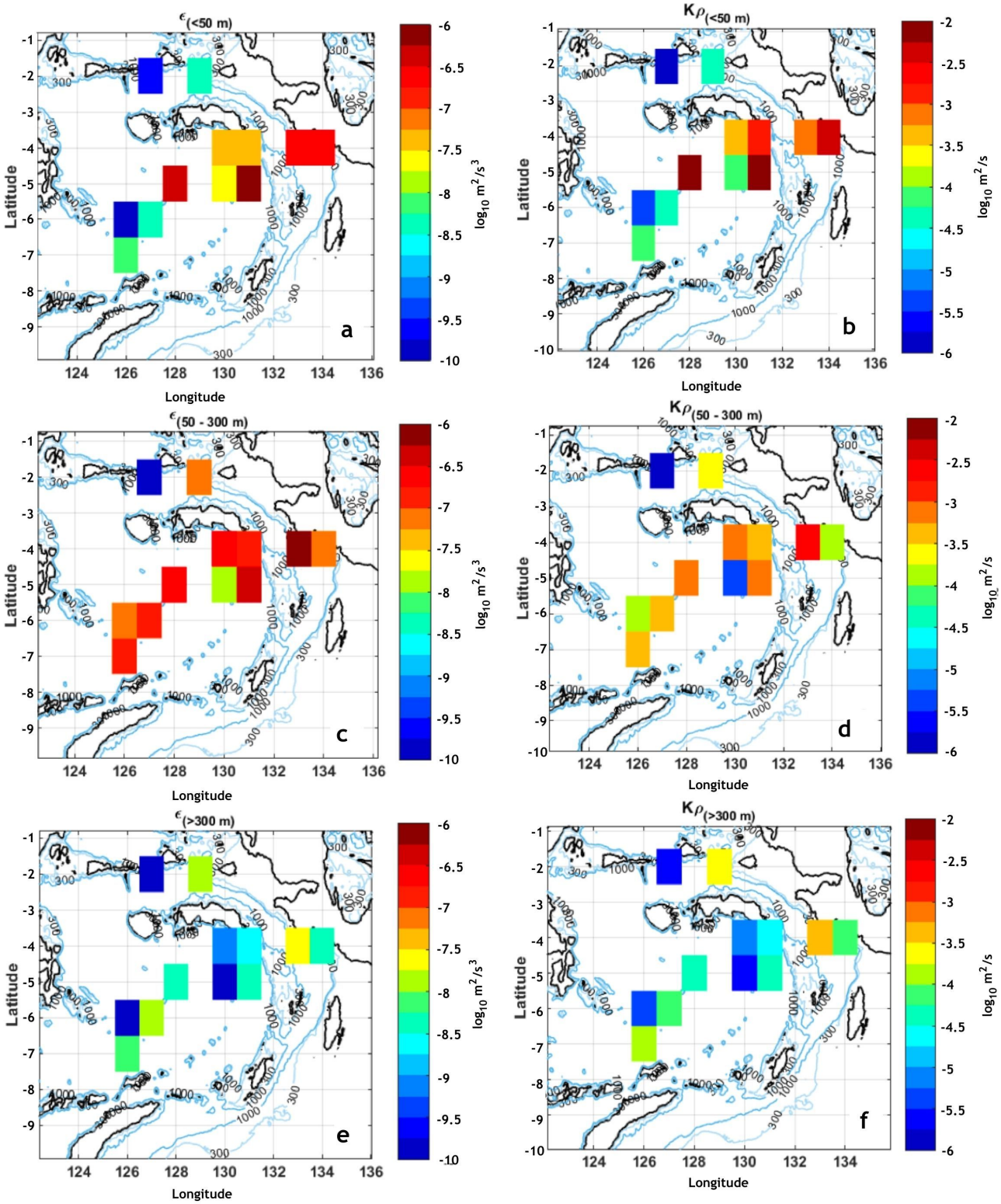


**Figure 8.** Average dissipation in different layers from JC II data; $\varepsilon$ ($\log 10\ m^2\ s^{-3}$) and $K_\rho$ ($\log 10\ m^2\ s^{-1}$). The topography was provided by GEBCO (General Bathymetric Chart of the Oceans).

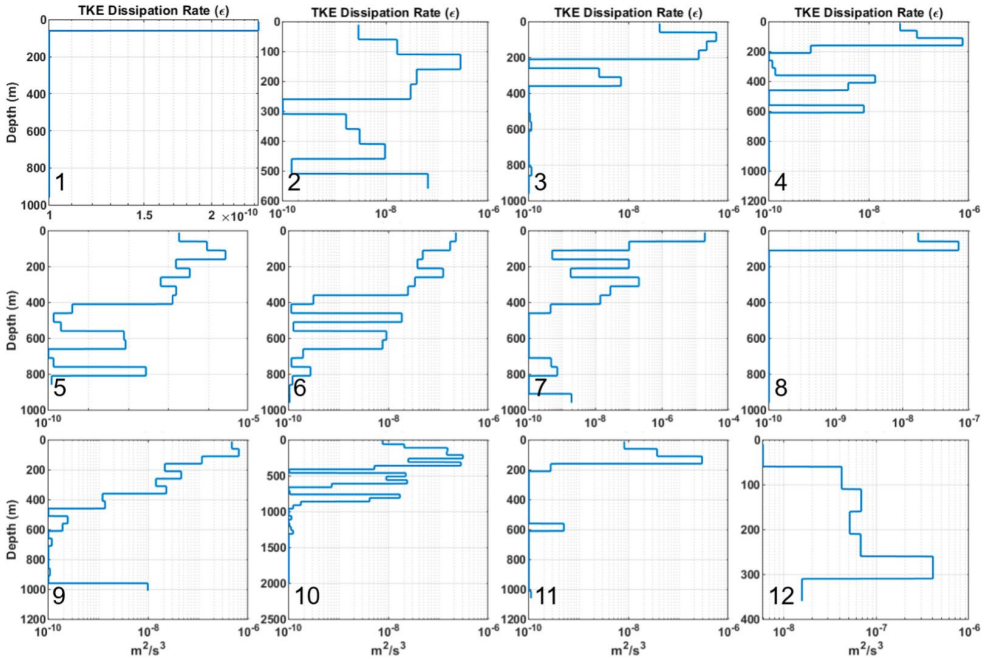


**Figure 9.** The vertical profile of turbulent kinetic energy dissipation rate ($\varepsilon = \mathrm{m}^2\ \mathrm{s}^{-3}$) from JC II data.

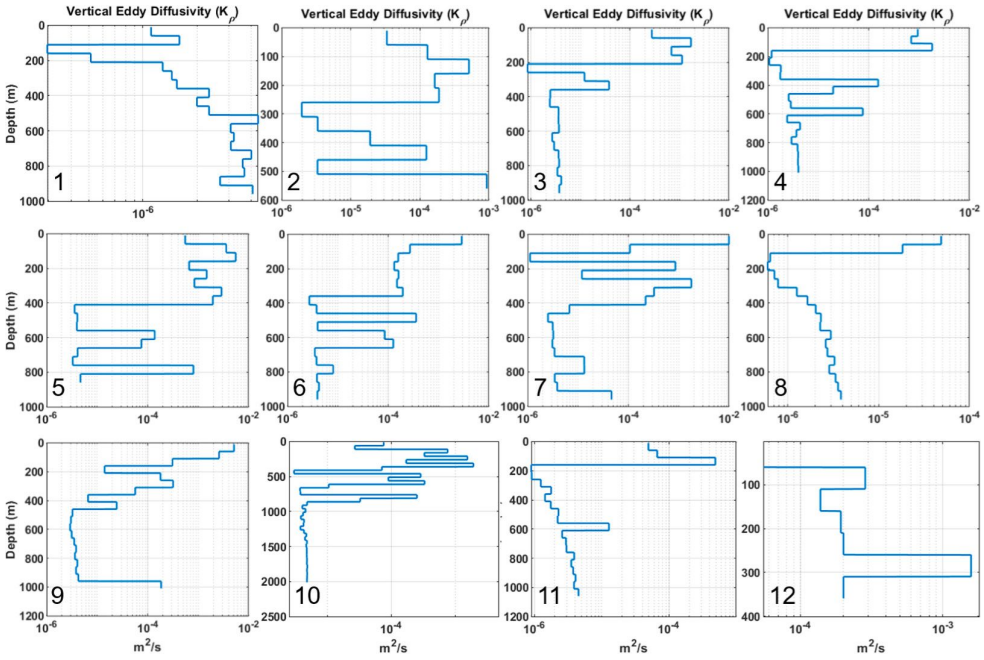


**Figure 10.** The vertical profile of eddy diffusivity from JC II data.

A similar pattern is observed in the vertical diffusivity profile $K_\rho$, where high diffusivity ($>10^{-4.5}$ m$^2$ s$^{-1}$) occurs at all stations in the mixed layer and thermocline. Furthermore, the highest diffusivity was observed at station 5 (northern Aru Sea) in the thermocline layer (50 to 180 m), with $K_\rho$ values ranging from $10^{-3}$ to $10^{-2.5}$ m$^2$ s$^{-1}$. This also indicated a linear relationship between the dissipation rate and diffusivity values. However, the diffusivity profile at stations 1 and 8 was inversely related to the dissipation rate profile, as the $K_\rho$ values at these stations range from $10^{-6}$ to $10^{-3.5}$ m$^2$ s$^{-1}$.

### 3.5 Particle movement tracking

The simulation results of particles movement in the Banda Sea during the same monsoon period indicate that the surface currents exhibit varied directions, but they are predominantly towards the southwest and western regions (Figure 11). Meanwhile, at 600 and 100 m, the particles

of water from all stations were in the same area during the simulation. For stations located in the Seram Sea (stations 1 and 2), the surface water particles movement is towards the south. The majority of water particles from stations located in the eastern Banda Sea (stations 3, 4, 5, 6, and 7) move westward, except for stations 3 and 6, which move northward and eastward, respectively. Water particles from stations located in the central Banda Sea (stations 8, 9, and 10) move westward with their paths remaining relatively parallel. Particles from station 9, situated further north than station 10, travel only as far south as Buru Island, whereas particles from stations 8 and 10 extend their movement further to Sulawesi. Water particles from stations located in the south of the Banda Sea (stations 11 and 12) move southward, passing through the Ombai Strait and into the Savu Sea. From the Savu Sea, the surface current parted into two directions: one heads directly towards the Indian Ocean, and the other flows towards the Timor Passage before eventually reaching the Indian Ocean. Within a one-month timeframe, the shortest distance is covered at station 6, which is located south of Papua, Indonesia, while the farthest distance is observed at station 10, which was initially situated in the middle of the Banda Sea, where the current reaches the Selayar Islands. The current at station 12 appears to form eddies due to the convergence of the current from station 10, resulting in a change in direction from northward to southward upon merging with the ocean currents at station 11.

In the simulation at a depth of 600 m, most particles tended to move east of the station. Stations 1 and 2 are situated in the Seram Sea, but the direction of movement is reversed: station 1 moved west and station 2 moved east. However, not all the particles in both stations move too far. In the eastern part of the Banda Sea for instance, stations 3, 4, 5, 6, and 7 movement is to the east, except for station 3, which moves westward toward the Maluku Islands. The movement of water particles in the center of Banda Sea comes from station 8, which is to the north. The displacement of particles coming from stations 9 and 10 is to the west, as well as at the surface, but over shorter distances. Water particles coming from the stations placed in the southern Banda Sea move directly to the east since the beginning of the simulation, in station 12, and first to the south before going towards the east in station 11. The most distant movement of particles at this depth is from station 12, and the shortest distance from station 2.

At depths of 1000 m, particle movements are also not too far from the release point in stations whose locations are in the Seram Sea and also in the central and eastern Banda Sea, while particles in stations that have places in the southern part of the Banda Sea will move further away. Due to the fact that the depth of the waters in both stations was less than 1000 m, station 2 in the Seram Sea and station 5 in the eastern part of the Banda Sea do not move at all. Water particles originating from station 1 in the Seram Sea run southward along the western coast of Buru Island. The trajectory path of the water particles in the eastern Banda Sea (stations 3, 4, 6, and 7) is to the west since the beginning, with the longest distance at station 3 and the shortest distance at station 6. Similar to the movement of water particles in the eastern part, stations located in the central Banda Sea also move westward, with the longest distance reaching station 9. The movement pattern of the water particles from the stations located in the southern Banda Sea is similar to their movement at a depth of 600 m. Station 11 first moved southward and then eastward, while station 12 moved directly to the east since the beginning of the simulation-with the longest range at station 12.

## 4. Discussions

In general, both data from the WOD-18 and JC II expeditions confirmed the findings of previous studies (Moore et al., 2003; Zhu et al., 2019; Zubaedah et al., 2021). In SEM, most of the Banda Sea has lower temperature due to an interchange of water masses from the Banda Sea, which results in a lower SST (Figure 3a). The accumulation of warm water in the center of the Banda Sea occurs in NWM (Figure 3b). This indicates a change in the Ekman current due to the monsoon, which results in differences in the movement of water masses and the Indonesian Throughflow (ITF) transport in NWM and SEM (Sprintall dan Timothy Liu, 2005). Furthermore, it is established that the Banda Sea is impacted by a pair of monsoon periods. Due to the prevailing winds, the northwest monsoon (December to February) triggers a current from the Flores Sea and Java Sea towards the Banda Sea. Conversely, the flow is reversed during the southeast monsoon (June to August). The waters from the Banda Sea move eastward through the Flores and Java Seas (Moore et al., 2003). In contrast, during the period of prevailing east monsoon winds (Australian monsoon), a pronounced movement of water masses occurs towards the Flores Sea and Java Sea (Purba et al., 2021). Meanwhile, the influx of water from the Pacific Ocean is insufficient. Consequently, water from the lower layers of the Banda Sea rises, a phenomenon known as the upwelling process (Birowo, 1984; Wyrtki, 1961). This circulation pattern is directly linked to the global oceanic mass circulation (ocean conveyor belt) (Ilahude et al., 1999). The process of upwelling observed in the Banda Sea during the eastern monsoon season, driven by the deficiency of water masses in the upper layers, reduces temperature and increases salinity. Banda Sea is a region which affected by the El Niño-Southern Oscillation (ENSO). However, the ENSO variability also influences the distribution of SST. The Oceanic Niño Index (ONI), the average SST anomaly in the Pacific Ocean (5°N–5°S, 120°W–170°W), in 2022 was consistently below −0.5°C which is a sign of the occurrence of La Niña. Stronger upwelling occurs because of La Niña, so the mass of water moving to the upper layers is more than usual (Pei et al., 2021). This resulted in lower

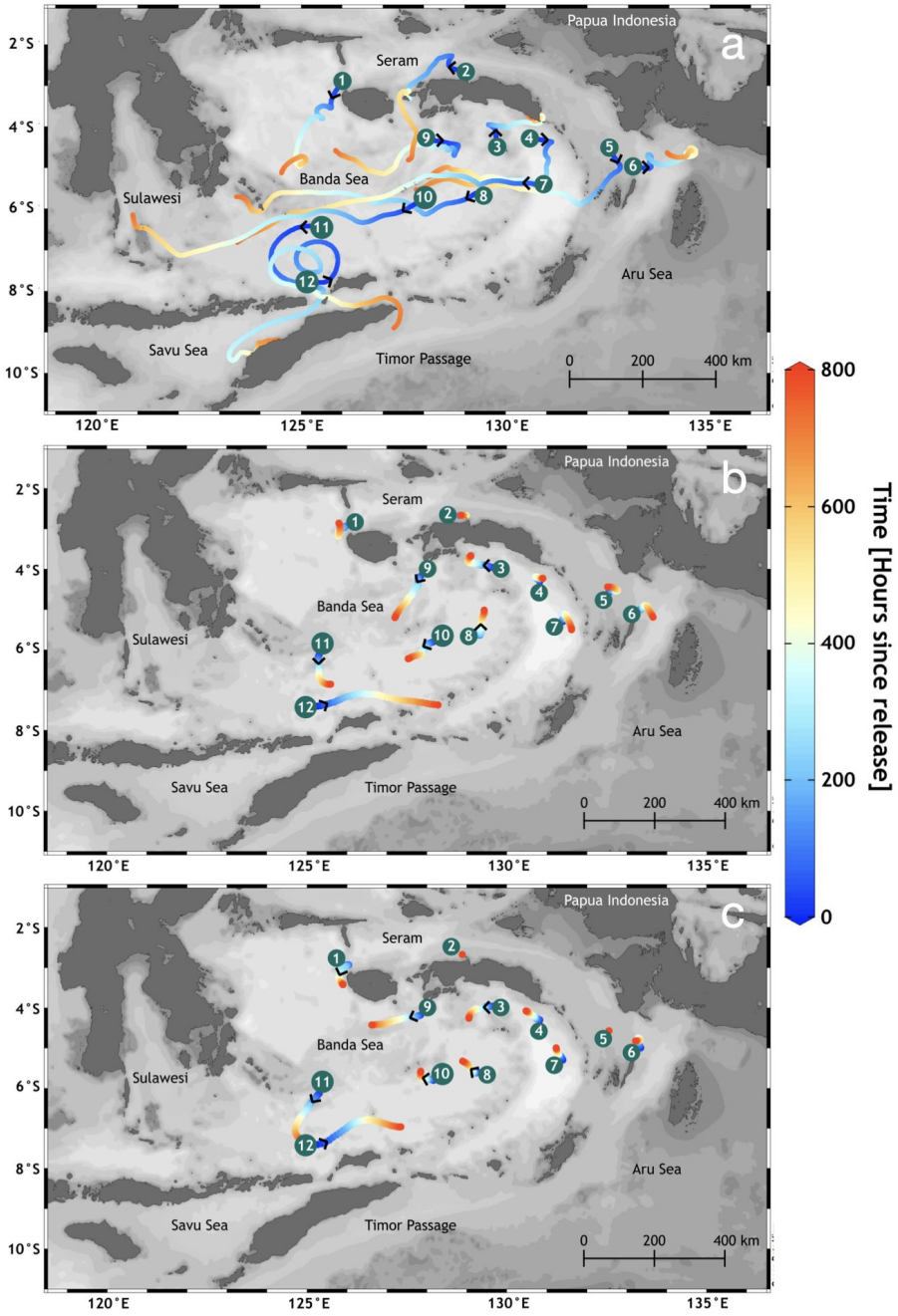


**Figure 11.** Particle pathways in the a) surface layer with start points from JC II stations, b) 600 m, and c) 1000 m

SST in SEM at AOI than it was 15 years ago, compared to SST (Horhoruw et al., 2020).

For salinity in the NWM, the highest value is found in the southern part of the Banda Sea (Figure 3c). This may be due to the presence of more saline water inputs coming from the Indian Ocean through several straits. Furthermore, there is a water mass that is less saline in the western part of the Banda Sea, which is a mass of water that comes from the Java Sea. The Java Sea is known as one of the regions that has many rivers and provides a lot of freshwater input to the sea. In the SEM season, higher salinity values can be seen in all areas (Figure 3d). In accordance with SST conditions, this season, there was an upwelling with strong intensity due to the wind blowing from Australia, which caused Ekman pumping (Purba et al., 2019). Another thing is that there are eddies that occur permanently in the Banda Sea, but in this figure, it is not clearly visible. Eddies found in the Banda Sea have the characteristics of anti-clockwise and clockwise patterns, which is a clockwise pattern carrying cold water masses (<26°C) in the lower layer upwards with the characteristics of colder water and higher salinity (>34.5).

The temperature in both seasons has almost the same characteristics in each layer (Figure 4a,b). In the upper layer, the mixing process occurs due to the presence of a monsoon. In the eastern part of the Banda Sea, the thermocline layer is shallower due to upwelling (Purba et al., 2019). The salinity from 150 m to deeper water in both monsoons has similar characteristics, which have a homogeneous layer of salinity found at about 400–900 m (Fieux et al., 1994; Molcard et al., 2001). During SEM, there are differences in the salinity, which varies with depth (Figure 4c). In the western regions, a salinity of 33.7 can be found at a depth of about 100 m, while in the eastern region, it can only be found at a depth of about 50 m. This happens as a result of water mass transfer, as described in the previous section. The upwelling process transports higher-salinity water in the eastern region to the surface, compensating for the displacement of water in the upper column (Vinayachandran et al., 2021). Meanwhile, in the SEM, it can be seen that the upper water layer has a lower salinity compared to the NWM (Figure 4d). The conditions were also similar to the results of the Jalacitra II expedition, which represents SEM (Figure 5). This shows that there is a similarity in profile both on the surface and the lower layer.

The upper limit of the thermocline layer that is often used is 20 isotherm (Tomczak and Godfrey, 2003). However, previous research found that Indonesian waters have a shallower thermocline layer than the equatorial Pacific, so the upper limit is the 22°C isotherm (Bray et al., 1996; Pusparini et al., 2017). Indonesian Upper Water (IUW) refers to the water in the upper thermocline of the ITF within the Indonesian seas (Talley and Sprintall, 2005). The salinity of IUW varies depending on location and depth. For instance, salinity ranges between 34.5 and 34.8 along the ITF pathway exiting the Indonesian waters across the mixed layer, thermocline, and intermediate layer (Makarim et al., 2019). In the ITF outflow region, the upper layer is dominated by Indian Ocean waters, while the lower layer is influenced by Pacific Ocean waters (Bayhaqi et al., 2018). Similar to IEW, IUW exhibits a temperature range of 8.0–23.0°C (Emery, 2015). Western North Pacific Central Water (WNCPW) is a water mass found in the northern Pacific Ocean, characterized by a temperature range of 10.0–22.0°C (Emery, 2015). WNCPW showcases salinity values spanning from 34.2 to 35.2 (Emery, 2015). This water mass constitutes part of the maximum salinity water (MSW) in the western North Pacific, distinguished by its unique salinity characteristics compared to other regions (Dippner et al., 2021). Intermediate Indonesian Water (IIW) is the sole water mass identified within the intermediate layer. It exhibits a temperature range of 3.5–5.5°C and a salinity of 34.6–34.7 (Emery, 2001). Salinity levels of IIW vary based on location and depth. Salinity remains relatively homogeneous in the eastern Timor region within the thermocline and intermediate layers (Atmadipoera et al., 2009). In the ITF outflow region, the upper layer is dominated by Indian Ocean waters, while the lower layer is influenced by Pacific Ocean waters (Bayhaqi et al., 2018).

The IIW and IUW are other significant water masses present in the region, including the Pacific Equatorial Water (PEW) and Eastern North Pacific Central Water (WNPCW), which are water masses that bring distinct characteristics and properties to the Indonesian seas, influencing the overall temperature, salinity, and circulation patterns. The temperature and salinity measurements in this study are similar to those of the ITF compared to previous research (Feng et al., 2018a; Gordon and Fine, 1996; Kida and Wijffels, 2012). The ITF in this region is categorized as a deep throughflow, as expounded by (Feng et al., 2018). Van Aken et al. (2009) analyzed salinity and temperature data along the eastern route of ITF (from Maluku to Seram to the Banda Sea). The deep throughflow of ITF is characterized by the transport of low thermocline waters from the Pacific into the Banda Sea and, ultimately, the Seram Sea (Gordon and Fine, 1996). The yo-yo measurements taken in June and August align with data from previous studies, leading to the conclusion that these yo-yo surveys encompass the ITF pathway in the Banda Sea region (Figure 6).

It is worth noting that the differences in water column stability between the two monsoons manifest in multiple dimensions (Figure 7). The spatial distribution across the east-west axis and the vertical distribution within the water column exhibit unique patterns during each monsoon. This variation results from the intricate interplay between wind patterns, ocean currents, and temperature-salinity dynamics specific to each monsoon season (Moore et al., 2003). This phenomenon indicates that the water column's stability responds differently to the distinct meteorological and oceanographic conditions associated with each monsoon. The dissimilarity in water column stability is evident when comparing the two monsoons. This discrepancy is noticeable not only across the lateral dimensions of the study area, particularly in the eastern and western zones but also in terms of the water column's vertical distribution.

High turbulence in the thermocline layer of the ocean has implications for mixing, nutrient transport, heat exchange, oxygenation, carbon cycling, vertical property transport, and upwelling/downwelling processes. In the Banda Sea, turbulence influences the formation and movement of ocean currents through several mechanisms (Figure 8). Turbulence enhances vertical mixing, disrupting density stratification and contributing to upwelling and downwelling currents formation. Additionally, turbulence affects the behavior of boundary currents, such as the Banda Sea Current, and influences the formation and dynamics of eddies, which play a role in transporting heat, nutrients, and other properties in the region.

Several factors could contribute to the occurrence of

low turbulence at stations 1 and 8. These factors include high thermal stability, little temperature difference between adjacent water layers, and relatively low current velocities. Additionally, the seafloor topography in the area and the interaction with other ocean currents can also influence turbulence levels. The absence of turbulence in the vertical dissipation rate profiles at stations 1 and 8 may be attributed to high thermal stability, low current velocities, and the specific location of these stations. The thermal stability reduces the transfer of mass and energy, thereby limiting the turbulence. The relatively low current velocities and possibly calm flow dynamics in the area also contribute to the lack of detectable turbulence in the dissipation rate profiles. Further analysis and specific observational data would be needed to understand better the reasons behind the low turbulence at stations 1 and 8. The highest turbulence is observed at station 5 in the thermocline layer (50 to 180 m), which is attributed to water mass outflow in the strait. Straits are known to be active turbulent regions due to higher tidal currents (Purwandana et al., 2020). In contrast, low turbulence is observed at stations 2 and 11, due to far from turbulence-generating sources.

Subsequently, surface currents exhibit different directions due to various factors such as wind, circulation influenced by the ITF, and the presence of islands (Zhu et al., 2019). During the JC II measurements, prevailing winds blew from Australia towards mainland Asia, resulting in a dominant westward surface current (Moore et al., 2003). A southward flow is also observed in the northern region, which is attributed to the presence of island contours. In the southern part of the Banda Sea, the presence of eddies was observed. These eddies are formed by the convergence of several currents, including those from the Java Sea and the Makassar Strait (Hanifah and Ningsih, 2016; Nuzula et al., 2017).

The simulations performed at depths of 600 m and 1000 m exhibited variations in speed and direction (Figure 11). The greatest distance is observed on the surface as a result of wind movement above sea level. The predominant flow direction on the surface, oriented towards the southwest and south, indicates the presence of the monsoon current and the Intertropical Convergence Zone (ITCZ) in this area. Currents emanating from stations 3 and 4 have altered their direction due to the confluence of currents from the northern region of Seram Island and the Banda Sea (Purba et al., 2021). Concurrently, station 1, situated in the southern region of Banda, encountered a phenomenon that may indicate the presence of eddies. At a depth of 600 m, the current's direction at station 12, located in the ITF outflow region, reaches its maximum distance of approximately 400 km to the east (Figure 11b). The eastern section (stations 4, 5, 6, 7) has a consistent pattern, indicating that the current direction in this area conforms to the seabed's contours. At station 10, the current is directed southwest and appears to converge with the trajectories of particles from stations 11 and 12. At this depth, the current pattern appears to conform to the geographical characteristics of the Banda Sea. The prevailing trend at a depth of 1000 m resembles that at 600 m, with the maximum distance recorded at station 12 (Figure 11c). The prevailing pattern in the central Banda Sea to the northwest exhibits a discrepancy with the top layer. This may result from the lack of wind, allowing the bottom current to prevail due to external pressures. Even though AAIW has a noticeable impact on the deep layer, further study is required to enhance our knowledge of the deep layer dynamics.

## 5. Conclusion

The result from the JC II Expedition confirmed the Banda Sea characteristic from the previous finding. The Banda Sea is situated within the Indo-Pacific region, which is known as a primary driver of global climate patterns. This study offers a comprehensive analysis of water mass transformations within the Eastern Indonesian Seas, drawing upon data from the World Ocean Database (WOD-18) and the recent JC II expedition. Understanding the characteristics of water masses and physical processes from the surface to the water column in the eastern Indonesian seas is key to studying various dynamics in Indonesian waters. Salinity characteristics at depths ranging from 150 meters to deeper layers during the Northwest Monsoon (NWM) and Southeast Monsoon (SEM). Nevertheless, significant salinity variations that emerged within the Surface Equatorial Mass (SEM) were consistent. Specifically, the western regions displayed a salinity of 33.7 at depths of approximately 100 meters, while the eastern region exhibited this salinity characteristic only at depths of around 50 meters. Furthermore, various water mass types found in this region include Bay of Bengal Water (BBW), Equatorial Intermediate Water (IEW), Indonesian Throughflow Upper Water (IUW), Western North Pacific Central Water (WNCPW), and Intermediate Indonesian Water (IIW). These characterizations provide valuable insights into these water masses' temperature and salinity ranges, thereby enhancing our understanding of their dynamics. The turbulence in the thermocline layer of the ocean in the Banda Sea has significant implications for various processes and phenomena. It influences mixing, nutrient transport, heat exchange, oxygenation, carbon cycling, vertical property transport, and upwelling/downwelling processes. Turbulence enhances vertical mixing, disrupts density stratification, contributes to the formation and dynamics of ocean currents, and influences the behavior of boundary currents and the formation of eddies. The occurrence of low turbulence at certain stations in the Banda Sea can be attributed to factors such as high thermal stability, minimal temperature differences between water layers, and relatively low current velocities. These factors limit the transfer of mass and energy,

reducing turbulence in those areas. Surface currents in the Banda Sea exhibit different directions due to wind patterns, the influence of the Indonesian Throughflow, and the presence of islands. Prevailing winds and the presence of islands contribute to the complex flow patterns observed, while the convergence of currents from the Java Sea and the Makassar Strait leads to the formation of eddies in the southern part of the Banda Sea. Meanwhile, the deep layer needs further analysis due to its different pattern from the surface and intermediate layer. The Banda Sea has the greatest biodiversity of species in the global ocean, and it is important to enhance our knowledge about the link between ocean condition and ecosystem.

## Funding

The research leading to these results received funding from Universitas Padjadjaran and the *Centre for Hydro-Oceanography, Indonesian Navy* (Pushidrosal), Jakarta, Indonesia.

## Acknowledgment

Universitas Padjadjaran and the *Centre for Hydro-Oceanography, Indonesian Navy* (Pushidrosal), Jakarta, Indonesia, supported and funded this study. The authors thank the Indonesian Chief of Hydrographer for the data used permit and the conference funding. We also thank the Captain of RV Rigel-933 for the support during the Jalacitra II-2022 "Banda" Expedition.

## Availability of data and materials

All data used are openly available and relevant websites are mentioned.

## Conflict of interest

None declared.

## References

Atmadipoera, A., Molcard, R., Madec, G., Wijffels, S., Sprintall, J., Koch-Larrouy, A., Jaya, I., Supangat, A., 2009. *Characteristics and variability of the Indonesian throughflow water at the outflow straits*. Deep Sea Res. Pt. I, 56 (11), 1942–1954. https://doi.org/10.1016/j.dsr.2009.06.004

Atmadipoera, A.S., Prartono, T., Jaya, I., Nugroho, D., Harsono, G., Nanlohy, P., Koch-Larrouy, A., 2019. *Seasonal variation of the upper-layer seawater properties in the Banda Sea: Observed from an autonomous CTD Argo float*. IOP Conf. Ser. Earth Environ. 278 (1). https://doi.org/10.1088/1755-1315/278/1/012008

Balsamo, G., Agusti-Panareda, A., Albergel, C., et al., 2018. *Satellite and in situ observations for advancing global earth surface modelling: A review*. Remote Sens. 10 (12), 1–72. https://doi.org/10.3390/rs10122038

Bayhaqi, A., Iskandar, I., Surinati, D., Budiman, A.S., Wardhana, A.K., Dirhamsyah, Yuan, D., Lestari, D.O., 2018. *Water mass characteristic in the outflow region of the Indonesian throughflow during and post 2016 negative Indian ocean dipole event*. IOP Conf. Ser. Earth Environ. 149 (1), 1–10. https://doi.org/10.1088/1755-1315/149/1/012053

Birowo, S., 1984. *Ekspedisi ilmiah kelautan Snellius II, Indonesia – Belanda (Juli 1984–Juli 1985)*. LIPI, Jakarta, 23–42.

Boyer, T.P., Baranova, O.K., Coleman, C., Garcia, H.E., Grodsky, A., Locarnini, R.A., Mishonov, A.V., Paver, C.R., Reagan, J.R., Seidov, D., Smolyar, I.V., Weathers, K.W., Zweng, M.M., 2018. *NOAA Atlas NESDIS 87*. World Ocean Database 2018.

Bray, N.A., Hautala, S., Chong, J., Pariwono, J., 1996. *Large-scale sea level, thermocline, and wind variations in the Indonesian throughflow region*. J. Geophys. Res. 101 (C5), 12239–12254. https://doi.org/10.1029/96JC00080

Cai, S., He, Y., Wang, S., Long, X., 2009. *Seasonal upper circulation in the Sulu Sea from satellite altimetry data and a numerical model*. J. Geophys. Res. 114 (3), 14. https://doi.org/10.1029/2008JC005109

Cheng, L., Zhu, J., Cowley, R., Boyer, T., Wijffels, S., 2014. *Time, probe type, and temperature variable bias corrections to historical expendable bathythermograph observations*. J. Atmos. Ocean. Tech. 31 (8), 1793–1825. https://doi.org/10.1175/JTECH-D-13-00197.1

Dippner, J.W., Weber, S.C., Subramaniam, A., 2021. *Impact of climate variability of the Western Tropical Pacific on maximum salinity water in the South China Sea*. Ocean. Dynam. 71 (10), 1033–1049.

Emery, W.J., 2015. *Oceanographic Topics: Water Types and Water Masses*. Enc. Atmos. Sci. 329–337. https://doi.org/10.1016/B978-0-12-382225-3.00279-6

Febriawan, H.K., Nugroho, A.B., Alodia, G., Hascaryo, A., Fadillah, A., Aryanto, N.C.D., Haryanto, D., Muljana, B., Endyana, C., Purba, N.P., 2023. *Nieuwerkerk – Emperor of China (NEC) Seamounts (Banda Sea): A multibeam seafloor imagery analysis*. IOP Conf. Ser. Earth Environ. 1163 (1), 012018. https://doi.org/10.1088/1755-1315/1163/1/012018

Feng, M., Zhang, N., Liu, Q., Wijffels, S., 2018. *The Indonesian throughflow, its variability and centennial change*. Geosci. Lett. 5 (1). https://doi.org/10.1186/s40562-018-0102-2

Fieux, M., Andrié, C., Delecluse, P., Ilahude, A. G., Kartavtseff, A., Mantisi, F., Molcard, R., Swallow, J.C., 1994. *Measurements within the Pacific-Indian oceans throughflow region*. Deep-Sea Res. Pt. I, 41 (7), 1091–1130.

Gordon, A.L., Fine, R.A., 1996. *Pathways of water between the Pacific and Indian oceans in the Indonesian seas*. Nature 379 (6561), 146–149.

Gusviga, B.H., Subiyanto, Faizal, I., Yusri, S., Sari, S. K., Purba, N.P., 2021. *Occurrence and Prediction of Coral Bleaching Based on Ocean Surface Temperature Anomalies and Global Warming in Indonesian Waters*. IOP Conf. Ser. Earth Environ. 750 (1), 1–13. https://doi.org/10.1088/1755-1315/750/1/012032

Hanifah, F., Ningsih, N.S. 2016. *The characteristic of eddies in the Banda Sea*. Adv. Appl. Fluid Mech. 19 (4), 889–902. https://doi.org/10.17654/FM019040889

Horhoruw, S.M., Fadli, M., Atmadipoera, A., Lekalette, J., Nugroho, D.Y., Tatipatta, W.M., Kainama, F. 2020. *Horizontal Structure of Banda Eddies and the Relationship to Chlorophyll-a during South East Monsoon in Normal and ENSO Period on 2008-2010*. IOP Conf. Ser. Earth Environ. 618 (1). https://doi.org/10.1088/1755-1315/618/1/012011

Ilahude, A.G., Muchtar, M., Praseno, D.P., Hadikusumah, A., Ruyitno, N., Simanjuntak, M., Sutomo, A.B., Adnan, Q. 1999. *Hydrology of the Mamberamo Plume, Irian Jaya*. Proc. Indo-Tropics Workshop, 6–7.

Jackett, D.R., McDougall, T.J., Feistel, R., Wright, D.G., Griffies, S.M., 2006. *Algorithms for density, potential temperature, conservative temperature, and the freezing temperature of seawater*. J. Atmos. Ocean. Tech. 23 (12), 1709–1728. https://doi.org/10.1175/JTECH1946.1

Johari, A., Akhir, M. F. 2019. *Exploring thermocline and water masses variability in southern South China Sea from the World Ocean Database (WOD)*. Acta Oceanol. Sin. 38, 38–47.

Johnson, G.C., Lyman, J.M. 2020. *Warming trends increasingly dominate global ocean*. Nat. Clim. Change 10 (8), 757–761. https://doi.org/10.1038/s41558-020-0822-0

Katavouta, A., Polton, J.A., Harle, J.D., Holt, J.T., 2022. *Effect of Tides on the Indonesian Seas Circulation and Their Role on the Volume, Heat and Salt Transports of the Indonesian Throughflow*. J. Geophys. Res. 127 (8). https://doi.org/10.1029/2022JC018524

Kida, S., Wijffels, S. 2012. *The impact of the Indonesian Throughflow and tidal mixing on the summertime sea surface temperature in the western Indonesian Seas*. J. Geophys. Res. 117 (C9).

Lana, A.B., Kurniawati, N., Purba, N.P., Syamsuddin, M.L. 2017. *Thermocline Layers Depth and Thickness in Indonesian Waters when Southeast Monsoon*. Omni Akuatika 37 (08), 36–41. https://doi.org/10.1002/jor.23509

Lange, M., van Sebille, E. 2017. *Parcels v0.9: Prototyping a Lagrangian ocean analysis framework for the petascale age*. Geosci. Model. Dev. 10 (11), 4175–4186. https://doi.org/10.5194/gmd-10-4175-2017

Liang, L., Xue, H., Shu, Y., 2019. *The Indonesian Throughflow and the Circulation in the Banda Sea: A Modeling Study*. J. Geophys. Res. 124 (5), 3089–3106. https://doi.org/10.1029/2018JC014926

Makarim, S., Sprintall, J., Liu, Z., Yu, W., Santoso, A., Yan, X.-H., Susanto, R.D., 2019. *Previously unidentified Indonesian Throughflow pathways and freshening in the Indian Ocean during recent decades*. Sci. Rep.-UK, 9 (1), 7364. https://doi.org/10.1038/s41598-019-43841-z

McCreary, J.P., Miyama, T., Furue, R., Jensen, T., Kang, H.W., Bang, B., Qu, T. 2007. *Interactions between the Indonesian Throughflow and circulations in the Indian and Pacific Oceans*. Progr. Oceanogr. 75 (1), 70–114. https://doi.org/10.1016/j.pocean.2007.05.004

Molcard, R., Fieux, M., Syamsudin, F., 2001. *The throughflow within Ombai Strait*. Deep-Sea Res. Pt. I 48 (5), 1237–1253.

Moore, T.S., Marra, J., Alkatiri, A. 2003. *Response of the Banda Sea to the southeast monsoon*. Mar. Ecol. Prog. Ser. 261, 41–49. https://doi.org/10.3354/meps261041

Nugraha, A.P., Purba, N.P., Junianto, Sunarto. 2018. *Ocean Currents , Temperature, and Salinity at Raja Ampat Islands and The Boundaries Seas*. World Sci. News 110 (September), 197–209.

Nuzula, F., Syamsudin, M.L., Yuliadi, L.P.S., Purba, N.P., Martono. 2017. *Eddies spatial variability at Makassar Strait – Flores Sea*. IOP Conf. Ser. Earth Environ. 54 (1). https://doi.org/10.1088/1755-1315/54/1/012079

Pei, S., Shinoda, T., Steffen, J., Seo, H., 2021. *Substantial Sea Surface Temperature Cooling in the Banda Sea Associated With the Madden-Julian Oscillation in the Boreal Winter of 2015*. J. Geophys. Res. 126 (6), e2021JC017226. https://doi.org/10.1029/2021JC017226

Purba, N.P., Damanik, F.S., 2021. *Seasonal Water Mass Transformation in Sulu and Surrounding Seas*. World Sci. News 153 (2), 142–156.

Purba, N.P., Khan, A.M.A., 2019. *Upwelling Session in Indonesia Waters*. World News Nat. Sci. 25 (June), 72–83.

Purba, N.P., Pranowo, W.S., Ndah, A.B., Nanlohy, P., 2021. *Seasonal variability of temperature, salinity, and surface currents at 0° latitude section of Indonesia seas*. Reg. Stud. Mar. Sci. 44, 101772. https://doi.org/10.1016/j.rsma.2021.101772

Purwandana, A., Cuypers, Y., Bouruet-Aubertot, P., Nagai, T., Hibiya, T., Atmadipoera, A.S., 2020. *Historical CTD dataset and associated processed dissipation rate using an improved Thorpe method in the Indonesian seas*. Data in Brief. 30. https://doi.org/10.1016/j.dib.2020.105519

Pusparini, N., Prasetyo, B., Ambariyanto, Widowati, I., 2017. *The Thermocline Layer and Chlorophyll-a Concentration Variability during Southeast Monsoon in the Banda Sea*. IOP Conf. Ser. Earth Environ. 55 (1), 012039. https://doi.org/10.1088/1755-1315/55/1/012039

Schlitzer, R., 2022. *Ocean Data View*. https://odv.awi.de

Sprintall, J., Gordon, A.L., Koch-Larrouy, A., Lee, T., Potemra, J.T., Pujiana, K., Wijffels, S.E., 2014. *The Indonesian seas and their role in the coupled ocean-climate system*. Nat. Geosci. 7 (7), 487–492. https://doi.org/10.1038/ngeo2188

Sprintall, J., Gordon, A.L., Wijffels, S.E., Feng, M., Hu, S., Koch-Larrouy, A., Phillips, H., Nugroho, D., Napitu, A., Pujiana, K., Dwi Susanto, R., Sloyan, B., Yuan, D., Riama, N. F., Siswanto, S., Kuswardani, A., Arifin, Z., Wahyudi, A.J., Zhou, H., Nagai, T., Ansong, J.K., Bourdalle-Badié, R., Chanut J., Lyard, F., Arbic, B.K., Ramdhani, A., Setiawan, A., 2019. *Detecting change in the Indonesian seas*. Front. Mar. Sci. 6, 257. https://doi.org/10.3389/fmars.2019.00257

Sprintall, J., Timothy Liu, W., 2005. *Ekman mass and heat transport in the Indonesian seas*. Oceanography 18 (Sp. Iss. 4), 88–97. https://doi.org/10.5670/OCEANOG.2005.09

Susanto, R.D., Fang, G., Soesilo, I., Zheng, Q., Qiao, F., Wei, Z., Sulistyo, B., 2010. *New surveys of a branch of the Indonesian throughflow*. T. Am. Geophys. Un. 91 (30), 261–263. https://doi.org/10.1029/2010EO300002

Talley, L.D., Sprintall, J., 2005. *Deep expression of the Indonesian Throughflow: Indonesian Intermediate Water in the South Equatorial Current*. J. Geophys. Res. 10 (10), 1–30. https://doi.org/10.1029/2004JC002826

Tillinger, D., Gordon, A.L,. 2009. *Fifty years of the Indonesian throughflow*. J. Climate, 22 (23), 6342–6355. https://doi.org/10.1175/2009JCLI2981.1

Tomczak, M., Godfrey, J.S., 2003. *Regional oceanography: an introduction*. Daya Books, New Delhi.

Van Aken, H.M., Brodjonegoro, I.S., Jaya, I., 2009. *The deep-water motion through the Lifamatola Passage and its contribution to the Indonesian throughflow*. Deep-Sea Res. Pt. I, 56 (8), 1203–1216.

Vinayachandran, P.N.M., Masumoto, Y., Roberts, M., Hugget, J., Halo, I., Chatterjee, A., Amol, P., Gupta, G., Singh, A., Mukherjee, A., Prakash, S., Beckley, L., Raes, E.J., Hood, R., 2021. *Reviews and syntheses: Physical and biogeochemical processes associated with upwelling in the Indian Ocean*. Biogeosciences Discuss. 18 (2), 5967–6029. https://doi.org/10.5194/bg-2020-486

Wyrtki, K., 1961. *Physical oceanography of the Southeast Asian waters*. Vol. 2, Univ. California, Scripps Inst. Oceanogr., California.

Zeng, L., Wang, D., Chen, J., Wang, W., Chen, R., 2016. *SCSPOD14, a South China Sea physical oceanographic dataset derived from in situ measurements during 1919–2014*. Sci. Data, 3 (1), 1–13.

Zhu, Y., Wang, L., Wang, Y., Xu, T., Li, S., Cao, G., Wei, Z., Qu, T., 2019. *Stratified Circulation in the Banda Sea and Its Causal Mechanism*. J. Geophys. Res. 124 (10), 7030–7045. https://doi.org/10.1029/2019JC015279

Zubaedah, S., Setiyono, H., Puspita, C.D., Gusmawati, N. F., Pranowo, W.S., 2021. *Schematic Model of Ocean Pacific Seawater Mass Circulation in Banda Sea*. IOP Conf. Ser. Earth Environ. 750 (1). https://doi.org/10.1088/1755-1315/750/1/012009